Proceedings of the XVII ECSMGE-2019
Geotechnical Engineering foundation of the future
ISBN 978-9935-9436-1-3

doi: 10.32075/17ECSMGE-2019-0871

XVII European Conference
ECSMGE 2019
Reykjavik
on Soil Mechanics
and Geotechnical Engineering

Effect of tangential surface load components on earth pressure coefficients

Effet des composants de charge de surface tangentielle sur les coefficients de pression de terre

N. Mortensen

nmGeo, Allerød, Denmark

A.Krogsbøll
nmGeo, Allerød, Denmark

ABSTRACT: Earth pressure coefficients for the ultimate limit state are usually derived considering the effect of vertical surcharge loading, the unit weight of soil and the effective cohesion as individual load components. This paper sets out the theoretical basis for adjusting the earth pressure coefficients when accounting for shear stresses along the retained soil surface, e.g. braking loads from trains. Focus has been given to the drained surcharge case. Corresponding results for the cases with effective cohesion and with the unit weight of soil have been discussed.

RÉSUMÉ: Les coefficients de pression terrestre pour l'état limite ultime sont généralement calculés en tenant compte de l'effet de la surcharge verticale, du poids unitaire du sol et de la cohésion effective en tant que composantes individuelles de la charge. Cet article expose les bases théoriques permettant d'ajuster les coefficients de pression terrestre lors de la prise en compte des contraintes de cisaillement le long de la surface du sol retenue, par ex. charges lors de freinage des trains. L'accent a été mis sur le cas d une surcharge drainée. Des résultats correspondants pour les cas ayant une cohésion efficace et avec le poids unitaire du sol ont été discutés.

Keywords: Zone ruptures; Shear stress; Braking load;

1 INTRODUCTION

Figure 1 is a geometrical representation of a soil that fails because of the wall, OA is being pushed towards the soil. Passive pressures are found when the wall moves towards the soil whereas active pressures reflect the wall moving away from the soil.

The scope of this paper is to investigate the change in the earth pressure when shear stresses acts along the soil surface.

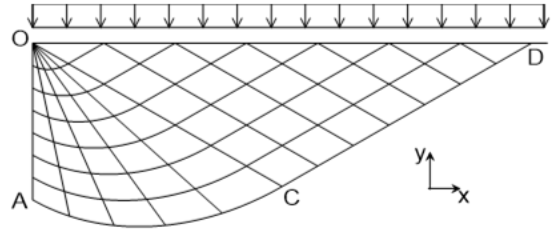

Figure 1. Passive failure in a weightless frictional soil behind a fully rough and vertical wall.

When dealing with earth pressure problems for a drained situation, three idealised contributions are usually investigated independently.

Each contribution has its own earth pressure coefficient (effective unit weight, γ' with K_γ, surcharge, p with K_p and effective cohesion, c' with K_c) and the unit earth pressure is found by $z \cdot \gamma' \cdot K_\gamma + p \cdot K_p + c' \cdot K_c$ where the term $z \cdot \gamma'$ is the vertical effective overburden pressure at the depth z and where the surcharge p is a vertical stress per unit of horizontal area.

In this paper, the theoretical basis for the surcharge case is given. The approach details the methodology from EN 1997-1, Annex C.2, which has been adopted from (Hansen 2001). The theoretical basis is extended to include the effect of shear stresses along the soil surface. The c'-case and the γ'-case have been included.

The basic assumptions applied are: **A)** the soil is homogeneous and isotropic, **B)** a failure within the soil can be described through a stiff-plastic drained Mohr-Coulomb failure criterion with φ' and c', **C)** the slip lines within the soil are considered as stress characteristics and **D)** all stress components and other parameters refer to an effective stress state.

2 VERTICAL SURCHARGE CASE

The earth pressure problem on Figure 1 includes a passive Rankine zone OCD and a Prandtl zone OAC. Boundary conditions along OD are outlined in Section 2.1 while Section 2.2 discusses the boundary conditions along the wall OA. Section 2.3 describes the derivation of the earth pressure coefficient.

2.1 Boundary condition at the soil surface

Figure 2 illustrates a small soil element in passive failure and where the element is bounded by the inclined soil surface and the slip lines (a-line and b-line) which are stress characteristics with the obtuse angle being defined by $\pi/2+\varphi'$.

The local t-n-coordinate system is rotated so the t-axis on Figure 2 coincides with the soil surface OD on Figure 1. Equations considering the boundary conditions at the soil surface refer to the local t-n-coordinate system, but these boundary conditions can be transformed to the global x-y-coordinate system once the value of m_t is known.

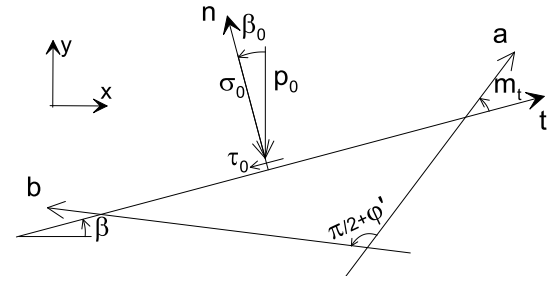

Figure 2. Soil element at soil surface drawn for a passive failure state using $\varphi' = 30°$ and $\beta = 10°$.

The value of p_0 on Figure 2 is the vertical surcharge per unit of surface area and σ_0 is the projection of p_0 on the local n-axis while τ_0 is the corresponding projection on the local t-axis. It may be shown that the stress components for a plastic failure state, relative to the t-n coordinate system, can be described by Equations (1)-(3), cf. (Hansen 2001):

$$\sigma'_t = \sigma'_v \, [1 + \sin\varphi' \sin(2m_t + \varphi')] \qquad (1)$$

$$\sigma'_n = \sigma'_v \, [1 - \sin\varphi' \sin(2m_t + \varphi')] \qquad (2)$$

$$\tau_{tn} = -\sigma'_v \sin\varphi' \cos(2m_t + \varphi') \qquad (3)$$

Where σ_v' is the mean effective stress, e.g. $(\sigma_x' + \sigma_y')/2$ with stress components referring to the x- and y-axis on Figure 2. From Figure 2 and Equation (2) it is seen that $\sigma_0 = \sigma'_n = p_0 \cdot \cos\beta_0$ and Equation (3) implies $\tau_0 = \tau_{tn} = p_0 \cdot \sin\beta_0$. Eliminating σ'_v leads to:

$$\cos(2m_t + \varphi' + \beta_0) = -\sin\beta_0 / \sin\varphi' \qquad (4)$$

Equation (4) allows for estimating the value of m_t directly. Setting $\sigma'_n = \sigma_0$ in Equation (2) leads to the mean effective stress in the soil element:

$$\sigma'_v = \sigma_0/[1 - sin\,\varphi'\,sin(2m_t + \varphi')] \qquad (5)$$

It may be proven that the slip lines within the Rankine zone are straight lines so the value of m_t is constant for the Rankine zone. The straight slip lines can be utilised to show that σ'_v within the Rankine zone is also constant. These conclusions are based on a weightless soil and a uniform surcharge.

2.2 Boundary conditions at the wall

Figure 3 shows a soil element in a passive failure and where the element is bounded by the wall and the a-line and b-line.

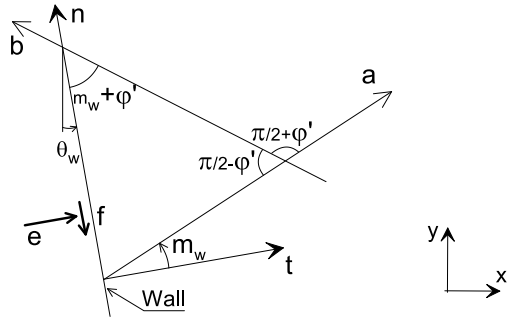

Figure 3. Soil element along the wall, drawn for a passive failure state. The symbols e and f represent the normal and the tangential components of earth pressures [unit of stress], respectively.

The local *t*-*n*-coordinate system is shown with the *n*-axis coinciding with the wall proper, which is inclined θ_w relative to vertical. The angle m_t on Figure 2 corresponds to the angle m_w on Figure 3, and the Equations (1) and (3) can thus be reformulated by replacing m_t with m_w as shown in the Equations (6) and (7):

$$\sigma'_t = \sigma'_v\,[1 + sin\,\varphi'\,sin(2m_w + \varphi')] = e \qquad (6)$$

$$-\tau_{tn} = \sigma'_v\ sin\,\varphi'\,cos(2m_w + \varphi') = f \qquad (7)$$

The last equality sign in the Equations (6) and (7) are seen directly from Figure 3. The sliding condition along the wall can be formulated using the Mohr-Coulomb failure criterion:

$$f = e\,tan\delta \qquad (8)$$

Where δ is the interface friction angle between the soil and the wall and where $|\delta| \leq |\varphi'|$.

Inserting Equation (6) and (7) into (8) leads to:

$$cos(2m_w + \varphi' + \delta) = sin\,\delta/sin\varphi' \qquad (9)$$

Equation (9) allows for estimating the value of m_w and the values of e and f can thus be found from Equations (6) and (7) directly.

2.3 Estimating the earth pressure coefficient

2.3.1 Statical and geometrical considerations

Section 2.1 concluded that the Rankine zone OCD on Figure 4 is characterised by straight a-lines and b-lines together with constant values of m_t and σ'_v.

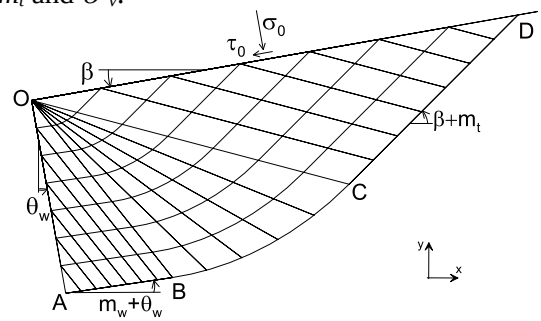

Figure 4. A passive surcharge case using $\varphi' = 30°$, $\delta = 20°$ with the wall and the soil surface inclined +10°.

The straight slip lines in the Rankine zone implies that the adjacent b-lines in the Prandtl zone OBC on Figure 4 also needs to be straight. Since the obtuse angle between an a-line and a b-line needs to be $\pi/2+\varphi'$, the a-lines within the Prandtl zone must be logarithmic spiral arcs with a characteristic angle of φ', and these arcs must have point O on Figure 4 as the pole point.

A wall zone OAB on Figure 4 will develop for a partly rough wall $0 < |\delta| < |\varphi'|$. The b-lines in the wall zone needs to be straight lines because of the straight b-lines in the Prandtl zone. Since the obtuse angle between the a- and b-lines need to be $\pi/2+\varphi'$, the a-lines have to be straight lines too.

If considering a smooth wall ($\delta = 0$) it is seen from Equations (4) and (9) that the angles m_w and m_t are alike and the Prandtl zone will vanish.

Independently of the value of δ, the angle between OB and OA on Figure 4 is $m_w+\varphi'$ (see also Figure 3) so the geometry of the wall zone OAB is defined when the height of the wall and the angle m_w are known.

Once the wall zone has been constructed, the Prandtl zone can be established by the polar equation for the logarithmic spiral arc:

$$R = R_0 \, exp(\theta \, tan\varphi')$$

Where the symbols are seen on Figure 5, representing the outer boundaries of the Prandtl zone OBC on Figure 4.

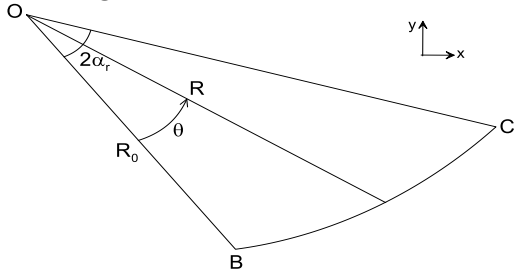

Figure 5. Logarithmic spiral arc reflecting the outer boundaries of the Prandtl zone on Figure 4.

The centre angle of the logarithmic spiral arc in the Prandtl zone is called $2\alpha_r$, cf. Figure 5, and the value can be found by geometrical conditions derived from Figure 4:

$$2\alpha_r = m_t - m_w + \beta - \theta_w \quad (10)$$

The value of $2\alpha_r$ must be non-negative for the Prandtl zone to be geometrically possible. The geometry of the failure mechanism is thus established.

2.3.2 Computational approach

Let σ'_C denote the mean stress within the passive Rankine zone OCD, and σ'_C can then be found by Equation (5). It may be shown that the value of a stress component changes along a logarithmic spiral arc, and from point C to point B the change can be described by:

$$\sigma'_C = \sigma'_B \, exp(4\alpha_r tan\,\varphi') \quad (11)$$

Since the wall zone has only straight slip lines, the stress components are constant within the zone, and σ'_B is thus the effective mean stress within OAB.

For the surcharge case we seek the relation $e = K_p \cdot p$. We know that $\beta_0 = \beta$ for the p-case, and we know that $\sigma'_0 = p_0 \cdot \cos\beta = p \cdot \cos^2\beta$, so combining the Equations (5), (6) and (11) implies:

$$K_p = K_1 cos^2\beta \quad (12)$$

Where:

$$K_1 = \frac{1+sin\,\varphi' \, sin(2m_w+\varphi')}{1-sin\,\varphi' \, sin(2m_t+\varphi')} \, exp(4\alpha_r tan\varphi') \quad (13)$$

The angles m_w, m_t and $2\alpha_r$ are estimated by the Equations (9), (4) and (10), respectively.

Positive values of φ' and δ shall be used when describing a passive failure by Equation (12), while negative values leads to an active failure.

K_c can be solved applying the p-case approach where σ_0 from Figure 2 is set to $c' \cdot \cot\varphi'$. The p-case is then solved assuming $c' = 0$ and the normal stress components are reduced by $c' \cdot \cot\varphi'$ before being used to establish the unit earth pressure.

For a horizontal surface the c'-case can be solved by the equation $K_c = (K_p - 1) \cdot \cot\varphi'$ by which K_c can be derived from K_p.

3 INCLINED SURCHARGE CASE

When looking at Figure 4, the soil surface is subjected to a normal stress σ_0 and a shear stress τ_0, which follows from an inclined soil surface, and τ_0 therefore vanishes when $\beta = 0$. Tangential surface load components are thus to be added separately in the equations in Section 2 and this can be introduced in different ways. The shear stress acting along the soil surface may be the only load present, meaning that a possible normal stress is zero. The shear stress will, however, often be linked to some sort of vertical loading, e.g. a braking load that will cause shear stresses along the soil surface, but the braking load will often be coupled with the weight of the braking vehicle. The effect of a shear stress is therefore introduced as illustrated on Figure 6.

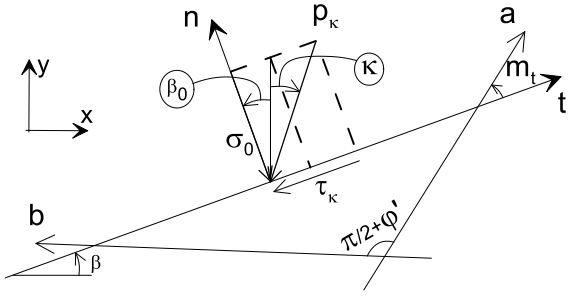

Figure 6. Soil element at soil surface.

Figure 6 resembles Figure 2. The load p_κ is the inclined surcharge per unit of surface area and $\sigma_0 = p_\kappa \cdot \cos(\beta_0+\kappa)$ is the projection of p_κ on the local *n*-axis while the projection on the local *t*-axis implies $\tau_\kappa = p_\kappa \cdot \sin(\beta_0+\kappa)$. Eliminating σ'_v when setting $\tau_\kappa = \tau_{tn}$ from Equation (2) and $\sigma_0 = \sigma'_n$ from Equation (3), leads to:

$$cos(2m_t + \varphi' + \beta_0 + \kappa) = -\frac{sin(\beta_0+\kappa)}{sin\,\varphi'} \quad (14)$$

Equation (14) represents a generalised version of Equation (4) where the estimated value of m_t in (14) accounts for the shear stress τ_κ. It is seen that $|\beta_0+\kappa| \leq |\varphi'|$. Equation (14) can also be obtained directly from Equation (4) when replacing β_0 in Figure 2 by $\beta_0+\kappa$ in Figure 6.

The value of K_p in Equation (12) must, however, also be updated to account for $\kappa \neq 0$:

$$K_{p,\kappa} = K_1 cos\beta\, cos(\beta + \kappa) \quad (15)$$

Where $K_{p,\kappa}$ is the earth pressure coefficient for the *p*-case including the effect of shear stresses along the soil surface, and where K_1 shall be estimated in accordance with Equation (13).

Section 2 can therefore be used to investigate the effect of tangential surface load components if Equations (4) and (12) are replaced by (14) and (15), respectively.

When the effect of shear stresses along the soil surface is included in the *p*-case, it shall not be included in the *c'*-case at the same time. It may, however, be left out in the *p*-case and included in the *c'*-case.

4 RESULTS

The methods described in the previous sections are applied to a vertical wall retaining soil with a horizontal surface. The results are presented as normalised values:

$$K_{norm} = \frac{K_{p,\kappa}}{K_{p,\kappa=0}} \quad (16)$$

$K_{p,\kappa}$ is estimated by Equation (15) ($\kappa \neq 0$) while $K_{p,\kappa=0}$ reflects Equation (12) ($\kappa = 0$). The value of K_{norm} can therefore be multiplied on K_p directly, provided that K_p has been estimated for similar assumptions as $K_{p,\kappa}$.

4.1 Passive surcharge case

Figure 7 shows the value of K_{norm} against κ for various values of φ' using a fully rough vertical wall for a passive case. Identical curves are found using a partly rough wall, which may be explained by the fact that K_{norm} is a normalised value. The nominator in Equation (16) is based on the same value of δ as the denominator, and

the normalised result K_{norm} seems to wash away the effect of δ.

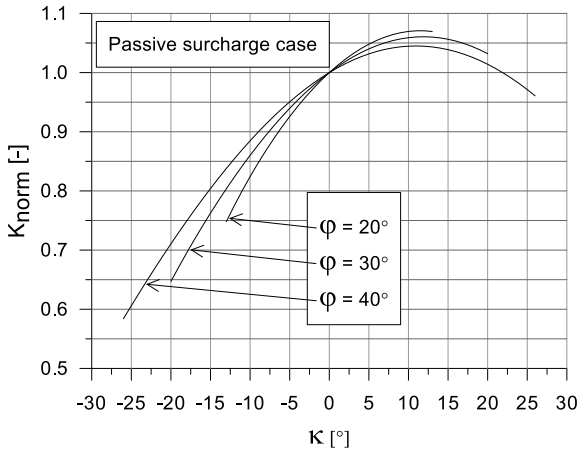

Figure 7. K_{norm} against κ for selected values of φ' assuming a passive failure for a vertical wall and a horizontal soil surface $\kappa \leq 2\varphi'/3$.

Assuming κ = +15° leads to an increase of approximately 5 % of the passive earth pressure coefficient, cf. Figure 7. Using κ = -15° leads to a reduction of approximately 20-25 %. Figure 8 depicts the extent of the Rankine and Prandtl zones for κ equal to +15°, 0° and -15° to illustrate the distorted Rankine zone caused by shear stresses along the soil surface.

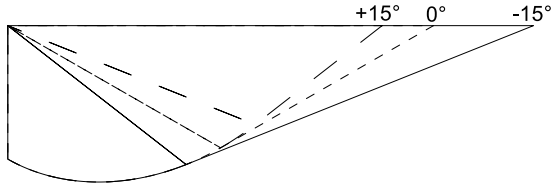

Figure 8. Bounding slip lines for $\varphi' = \delta = 30°$ and for selected values of κ.

Curves in line with the ones on Figure 7 have been estimated using an inclined soil surface but there seems to be no strong correlation between κ and β.

4.2 Active surcharge case

Figure 9 is based on an active case but using similar assumptions as for Figure 7.

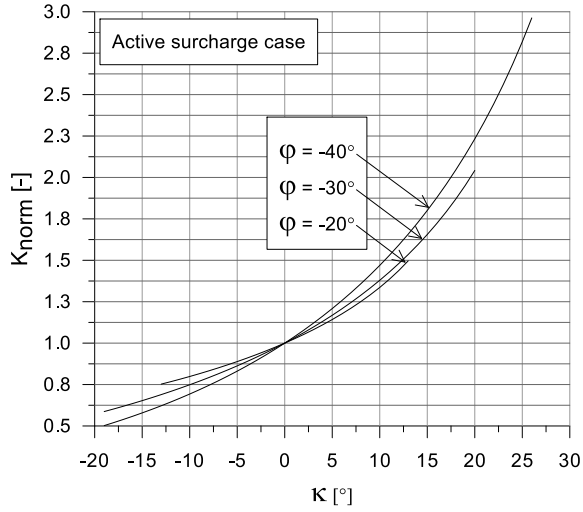

Figure 9. K_{norm} against κ for selected values of φ' assuming an active failure for a vertical wall and a horizontal soil surface $\kappa \leq 2\varphi'/3$.

As found for the passive case in Figure 7, the curves on Figure 9 do not change when using a partly rough wall.

A possible link between the value of κ and the value of m_t (Figure 6) was investigated. The angle m_t tends to reach 90° when κ gets lower than approximately -20° almost independently of φ', which indicates that a different failure type will develop instead of the investigated type.

Figure 9 shows that for κ = +15°, the active earth pressure coefficient is approximately 80 % higher than the value found for κ = 0.

Figure 10 depicts the extent of the Rankine and Prandtl zone for κ = -15°, 0° and +15° to show the variation in the rupture figure.

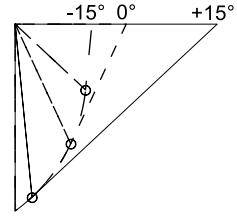

Figure 10. Bounding slip lines for $\varphi' = \delta = -30°$ and for selected values of κ.

Figure 10 includes three small circles each placed on the lowest point of the Rankine zone

(point C on Figure 4). For κ = -15° the angle m_t is close to 90° and the extent of the Rankine zone is limited. For κ = +15° the extent of the Rankine zone is rather significant.

5 UNIT WEIGHT CASE

If only shear stresses are added along the soil surface for the pure γ'-case, the soil will fail unless normal stresses are included. This means that shear and normal stresses must be combined in the same case and this is covered by the surcharge case. The γ'-case shall therefore not be corrected for possible shear stresses along the soil surface.

In the γ'-case, the a- and b-lines are curved, so a closed form expression cannot be established, and numerical integration must be applied. For a bearing capacity problem, the γ'-case was solved by (Lundgren & Mortensen 1953) and the primary author of the present paper used the same technique to estimate the earth pressure coefficient, K_γ. The active earth pressure coefficient for the γ'-case can be set equal to that of the p-case without introducing any real approximations.

Equations (18) and (19) are approximations to the passive K_γ from (Mortensen 1995) and (Lundgren & Hansen 1965), respectively.

$$K_\gamma^{KM} = K_p/cos\delta \tag{18}$$

$$K_\gamma^{LH} = K_p + 0.007(e^{9sin\delta} - 1) \tag{19}$$

Where K_p is the earth pressure coefficient from the p-case, estimated using the δ-value in question.

Figure 11 shows a slashed area marked with K_γ^{KM} / K_γ being based on Equation (18). The lower bound curve of the slashed area is the minimum value of the ratio K_γ^{KM} / K_γ for a given friction angle, allowing δ to vary between φ'/3 and φ'; the Equations (18) and (19) are exact for a smooth wall. The upper bound curve represents the maximum value of the same range in δ. The slashed area therefore shows the accuracy of the approximation to K_γ. The similar range is shown for K_γ^{LH} / K_γ. The figure also shows the ratios estimated for $\delta = 2\varphi'/3$.

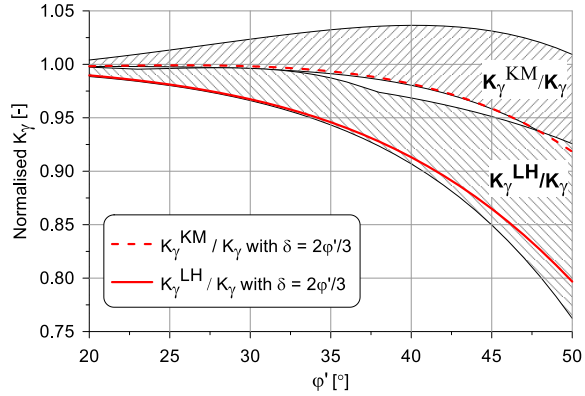

Figure 11. Normalised evaluation of Equation (18) and (19) against φ' using a vertical wall and a horizontal soil surface together with κ = 0.

Figure 11 shows that Equation (18) do not deviate more than 4 % from the theoretically correct value provided that $\varphi' \leq 45°$. Equation (18) is probably the most simple and accurate approximation to the theoretical value of K_γ for the passive case.

6 DISCUSSIONS

If referring to Eurocode EN 1991-2, the characteristic value of the lateral braking load of a train is approximately 25 kN/m, while the corresponding vertical load from Load Model 71 is either 80 kN/m or 156 kN/m with the latter representing the effect from concentrated axels. The resulting surcharge load is thus inclined by κ = +9° or +17° = atan(25/80).

If the horizontal rails pass a tunnel established in a frictional fill with a design value of φ' = 30°, the effect of κ = +9° (or 156 kN/m) implies that the active pressure from surcharge on the tunnel wall should be increased by a factor of 1.33 relative to κ = 0°, cf. Figure 9. For the 17° load inclination, the corresponding factor is 1.79 (80 kN/m).

The resulting effect is therefore that the load from the load case with the largest vertical line load is further increased with an additional factor on the surcharge part being approximately equal to the partial factor on the load itself.

This conclusion relies on the braking load being resisted by lateral shear stresses in the soil below the footprint area of the train. The rails may distribute the braking load to areas outside the footprint area of the train causing κ to decrease but the passive resistance on the other side of the tunnel would thus reduce, cf. Figure 7.

When evaluating the value of $K_{p,\kappa}$ for a given case, a simpler approach can be considered. Figure 12 assumes that an active earth pressure coefficient can be estimated by 1 - sinφ', and the safe zone on Figure 12 reflects that 1-sin$\varphi' \geq K_{p,\kappa}$ where $K_{p,\kappa}$ has been estimated by Equation (15). Figure 12 hereby shows when (1-sinφ') is unsafe.

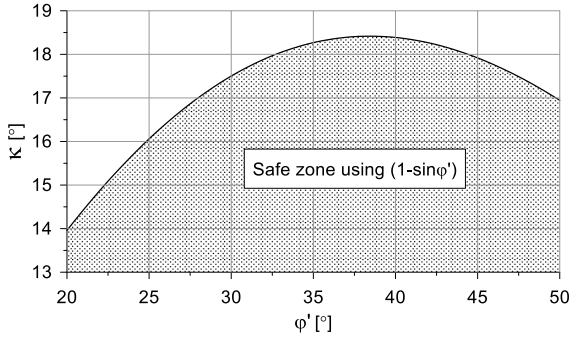

Figure 12. Estimated link between φ' and κ assuming (1-sinφ') = $K_{p,\kappa}$ for an active case using a horizontal soil surface and a vertical wall.

7 CONCLUSIONS

The theoretical basis for deriving the traditional earth pressure coefficients for the *p*-case has been given and procedures for the *c'*-case are sketched. For the γ'-case it has been suggested that the active state may be modelled by the active earth pressure coefficient from the *p*-case, while the passive γ'-case should be found from Equation (18).

When introducing shear stresses along the soil surface, the *p*-case should be adjusted to reflect the change in boundary condition, whereas the γ'-case and the *c'*-case should not. Graphs have been included to aid this adjustment.

The passive surcharge pressure increases by approximately 5 % whereas the active surcharge pressure increases by approximately 80 % when the shear stresses act towards the retaining wall depending on the value of the shear stress in question.

8 ACKNOWLEDGEMENTS

The authors are very grateful for the financial compensation made available by the company nmGeo, making this paper possible.

9 REFERENCES

Hansen, B. 2001, Advanced theoretical soil mechanics, Bulletin 20, The Danish Geotechnical Society, ISBN 87-89833-11-2

Lundgren, H. & Hansen, J.B. (1965): Geoteknik, 2. edition, Teknisk Forlag, København 1965.

Lundgren, H. & Mortensen, K. (1953): Determination by the Theory of Plasticity of the Bearing Capacity of Continuous Footings on Sand, Proceedings 3rd International Conference on Soil Mechanics & Foundation Engineering, Vol. 1, p. 409-412, Zürich 1953.

Mortensen, K. (1995): Kinematically and statically plausible calculations for sheet walls, Canadian Geotechnical Journal, Volume 32, No 3, 1995.